TISSUE ENGINEERING: Part C
Volume 16, Number 3, 2010

DOI: 10.1089/ten.tec.2009.0185

In Vivo Acceleration of Skin Growth Using a Servo-Controlled Stretching Device

Michael S. Chin, M.D.,[1,2] Rei Ogawa, M.D., Ph.D.,[1,3] Luca Lancerotto, M.D.,[1,4] Giorgio Pietramaggiori, M.D., Ph.D.,[1,4] Kevin T. Schomacker, Ph.D.,[5] Jasmine C. Mathews, M.A.,[1,2] Saja S. Scherer, M.D.,[1] Paul Van Duyn, B.S.,[6] Michael J. Prsa, B.S.,[6] Mark P. Ottensmeyer, Ph.D.,[7] Aristidis Veves, M.D., D.Sc.,[8] and Dennis P. Orgill, M.D., Ph.D.[1]

Tension is a principal force experienced by skin and serves a critical role in growth and development. Optimal tension application regimens may be an important component for skin tissue engineering and dermatogenesis. In this study, we designed and tested a novel servo-controlled skin-stretching device to apply predetermined tension and waveforms in mice. The effects of static and cyclical stretching forces were compared in 48 mice by measuring epidermal proliferation, angiogenesis, cutaneous perfusion, and principal growth factors using immunohistochemistry, real-time reverse transcriptase–polymerase chain reaction, and hyperspectral imaging. All stretched samples had upregulated epidermal proliferation and angiogenesis. Real-time reverse transcriptase–polymerase chain reaction of epidermal growth factor, transforming growth factor β1, and nerve growth factor demonstrated greater expression in cyclically stretched skin when compared to static stretch. Hypoxia-induced factor 1α was significantly upregulated in cyclically stretched skin, but poststretch analysis demonstrated well-oxygenated tissue, collectively suggesting the presence of transient hypoxia. Waveform-specific mechanical loads may accelerate tissue growth by mechanotransduction and as a result of repeated cycles of temporary hypoxia. Further analysis of mechanotransduction signaling pathways may provide additional insight to improve skin tissue engineering methods and optimize our device.

Introduction

Mechanical forces play a crucial role in normal skin growth during human development and facilitate the formation of three-dimensional structures. Shear,[1] tension,[2] compression,[3,4] and hydrostatic pressure[5,6] are conducted through the extracellular matrix or extracellular fluid to individual cells. It has been proposed that cells convert these mechanical stimuli into electrical signals through mechanoreceptors (mechanosensors) such as mechanosensitive ion channels,[7] cell adhesion molecules including integrins, and actin filaments in the cytoskeleton.[8–10]

We have focused recent studies on the application of mechanical forces for skin tissue engineering and dermatogenesis.[11,12] To accelerate skin growth, we have been developing skin-stretching strategies and devices. Tension is a principal force experienced by skin, and the optimal amplitude and waveform may facilitate the growth and expansion of skin. We previously applied static and periodic tensile forces to rat ears and showed vascular remodeling and epidermal proliferation.[11] A gene chip analysis performed on this rat model suggested hypoxia at the tissue level as a possible mechanism for the observed effects.[13] In addition, prior *in vitro* studies have shown that mechanotransduction mechanisms stimulate cell proliferation[14] and angiogenesis.[15,16]

In this study, we designed and tested a novel stretching device on dorsal murine skin to accelerate tissue growth by repeatedly stimulating mechanotransduction and hypoxic

[1]Tissue Engineering and Wound Healing Laboratory, Division of Plastic Surgery, Brigham and Women's Hospital, Harvard Medical School, Boston, Massachusetts.
[2]Division of Plastic Surgery, University of Massachusetts Medical School, Worcester, Massachusetts.
[3]Department of Plastic, Reconstructive, and Aesthetic Surgery, Nippon Medical School, Tokyo, Japan.
[4]Clinic of Plastic Surgery, University of Padova, Italy.
[5]HyperMed Inc., Burlington, Massachusetts.
[6]Wentworth Institute of Technology, Boston, Massachusetts.
[7]Simulation Group, CIMIT, Massachusetts General Hospital, Boston, Massachusetts.
[8]Joslin-Beth Israel Deaconess Foot Center and Microcirculation Laboratory, Beth Israel Deaconess Medical Center, Harvard Medical School, Boston, Massachusetts.

pathways. Dorsal murine skin does not have the cartilage that complicated our stretching analysis in the rat ear[11] and allows for the wide range of experimental designs available to murine models. This device was servo-controlled and capable of reliably applying specified tensile forces and waveform patterns to skin.

Materials and Methods

Design and analysis of skin-stretching device

Design of skin-stretching device. The computer-controlled device (Fig. 1A) consisted of a lightweight distractor moved by a 6 mm stepper motor (ADM0620-V3-05; Arsape, La-Chaux-de-Fonds, Switzerland) coupled to a planetary gear (Series 06/1, 256:1 gear ratio; Arsape) and rack-and-pinion drive (0.4 module, 20° pressure angle rack with 6 mm pitch diameter pinion; SDP-SI, New Hyde Park, NY). The rack moved 3.68 μm per motor step with a maximum force of 1.22 kgf, although much lower forces were used in this study. Two removable feet were added under the arms of the distractor to conform to the shape of the mouse dorsum. The entire motor–distractor assembly had a mass of approximately 27 g, but much of this load was supported by tethering the device wires.

The voltage output of a bar-shaped load cell (S215; Strain Measurement Devices, Meriden, CT) was amplified (instrumentation amplifier chip INA125; Burr-Brown/Texas Instruments, Dallas, TX) and processed by a USB-1208LS Data Acquisition Controller (12-bit resolution; Measurement Computing, Norton, MA) yielding a resolution of 0.08 gram-force (gm-f) per bit.

LabVIEW 7.1 (National Instruments, Austin, TX) was used for data acquisition and closed loop force control of the distractor, offering the possibility of applying constant or cyclical tensile stimulation with adjustable parameters such as the shape of the force waveform, the length of the phases of cycles, the intensity of applied forces, and the number of cycles. A bang-bang controller running at 1 kHz was implemented, yielding a maximum distraction speed of 3.68 mm/s. Signal intensities were automatically logged into a spreadsheet for later analysis (Excel Microsoft Corporation, Redmond, WA).

Finite element analysis of stretching force. We modeled mouse skin as a three-dimensional solid representation of a homogeneous, isotropic, linearly elastic material (Young's modulus of elasticity [E] of 400,000 N/m^2 and a Poisson's ratio [v] of 0.49) using FEMLAB 3.1 (Comsol, Paris, France).

A 4.0×3.0×0.1 cm section of skin was modeled with a square (1 cm^2) area representing the center of the mouse dorsum. Two regions corresponding with the adhesive pads (labeled A and B in Fig. 1B) were added, creating a composite object. The outside boundaries of the composite were left unconstrained, corresponding with the loose skin of the actual mouse dorsum. Serial 2, 4, and 6 mm displacements were imposed on pads A and B along the horizontal axis. The model was solved for tissue displacement, reaction force, strain distribution, as well as principal and von Mises stress distributions.

Device attachment sensor feedback, and macroscopic analysis. The dorsum of each mouse was clipped 24–72 h before each experiment and a 1-cm-wide×5-cm-long transverse strip was depilated (Nair; Church & Dwight, Princeton, NJ). Mice were anesthetized with an intraperitoneal injection of 60 mg/kg pentobarbital (Nembutal Sodium Solution; Abbot Laboratories, Abbott Park, IL) 10 min before application of the device. To verify force sensor calibration before testing, a reading was taken with a 50 g mass suspended from the sensor corresponding with the peak tensile load commanded during the experiments. The feet were then positioned 1 cm apart. A layer of paper tape was attached underneath each foot of the device and glued to the skin of the dorsum caudally and rostrally to the designated 1 cm^2 skin area using 2-octyl cyanoacrylate surgical glue (Dermabond; Ethicon, Somerville, NJ).

To examine the reliability of the actual force applied to the dorsal skin, the sensor logs were analyzed. Force amplitude was recorded at intervals of 1.5 s. Samples that did not follow the specified parameters were omitted from the study. Digital photos were taken before and after application of the devices and examined for macroscopic evidence of tissue damage.

In vivo *skin stretching and analysis of stretched skin*

Experimental design. A total of 48 adult male wild-type C57Bl6 *db*/+ mice (Jackson Laboratory, Bar Harbor, ME) were housed in an Association for Assessment and Accreditation of Laboratory Animal Care–certified facility under an approved experimental protocol. Thirty mice were used for immunohistochemistry, 6 mice for real-time reverse transcriptase–polymerase chain reaction (RT-PCR), and 12 mice were used for hyperspectral imaging study (Fig. 1C).

Immunohistochemistry. Vessel number, epidermal proliferation, and inflammation were analyzed by immunohistochemistry using 30 mice assigned to five different groups. Two groups of mice were subjected to a cyclical square-wave tensile stimulation for 1 and 4 h, respectively, using a pattern of 2 min on (50 gm-f)/1 min off (0 gm-f). The third group and fourth group underwent static stimulation of 50 gm-f amplitude for 1 and 4 h. The fifth group served as a control and underwent 4 h with the device attached as described above,

FIG. 1. (**A**) The stretch device was constructed from a lightweight stepper motor/planetary gear system (A), a rack and pinion transmission (B), and a bar-shaped load cell (C). (**B**) Finite element analysis. Serial von Mises stress plots predicted nearly uniform stress distribution along the mid-place (indicated as a vertical line) and increasing tension between adhesive pads A and B when they were displaced by 2, 4, and 6 mm in the x-direction. Units are in pascals. (**C**) Overview of study timeline. Application of skin stretch was performed on day 0. HSI was performed on days 0–3. Mice were sacrificed for immunohistochemical staining on days 2 and 3. RT-PCR for *EGF, VEGF,* and *HIF-1α* was performed on day 2. (**D**) Examples of sensor feedback readings. Yellow lines represent the desired pattern for each stimulation. (Left) 1 h cyclical stretch. (Right) 1 h static stretch. HSI, hyperspectral; RT-PCR, reverse transcriptase–polymerase chain reaction; *EGF,* epidermal growth factor; *VEGF,* vascular endothelial growth factor; *HIF-1α,* hypoxia-induced factor 1α. Color images available online at www.liebertonline.com/ten.

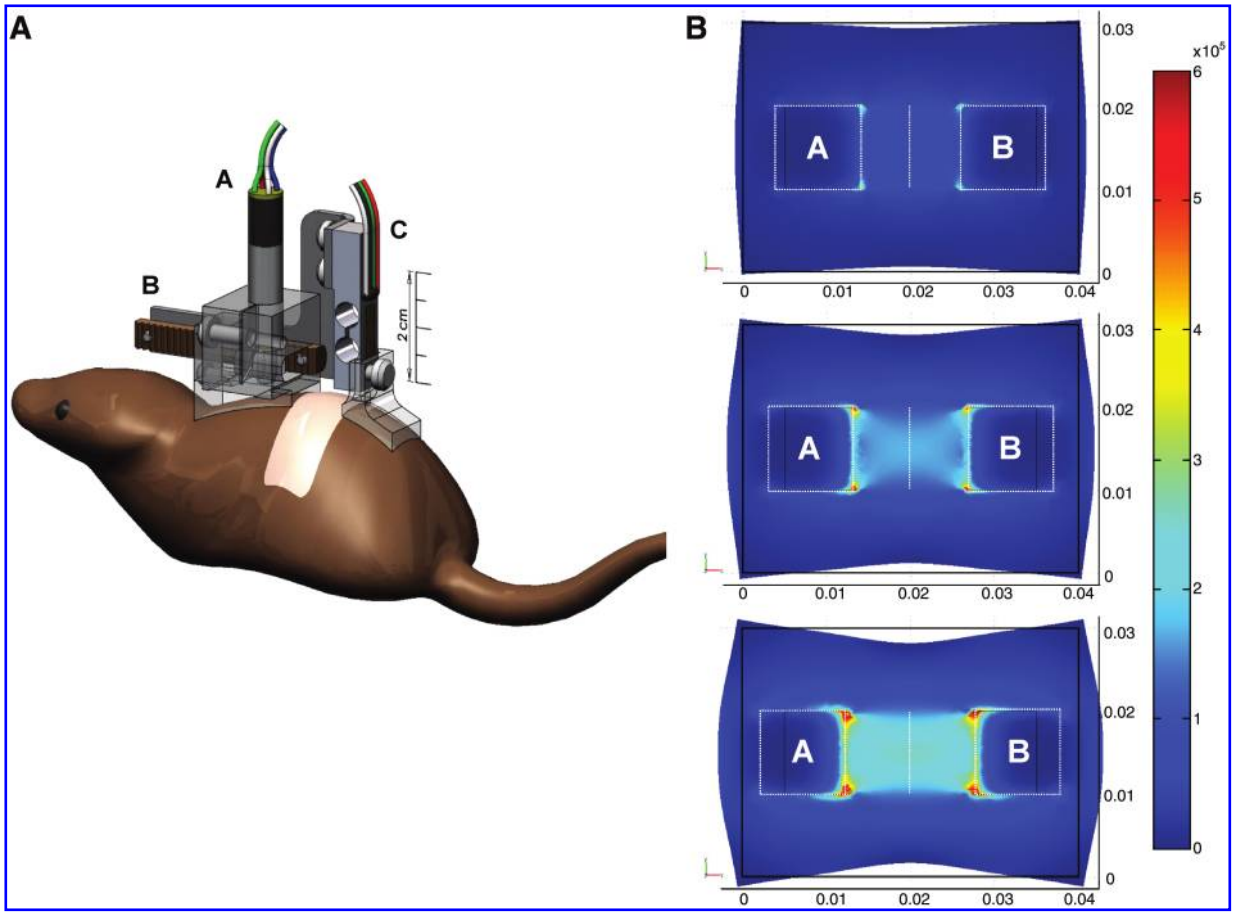
A
A
B
C
2 cm
B
A
B
0.03
0.02
0.01
0
0.01
0.02
0.03
0.04
x10^5
6
5
4
3
2
1
0

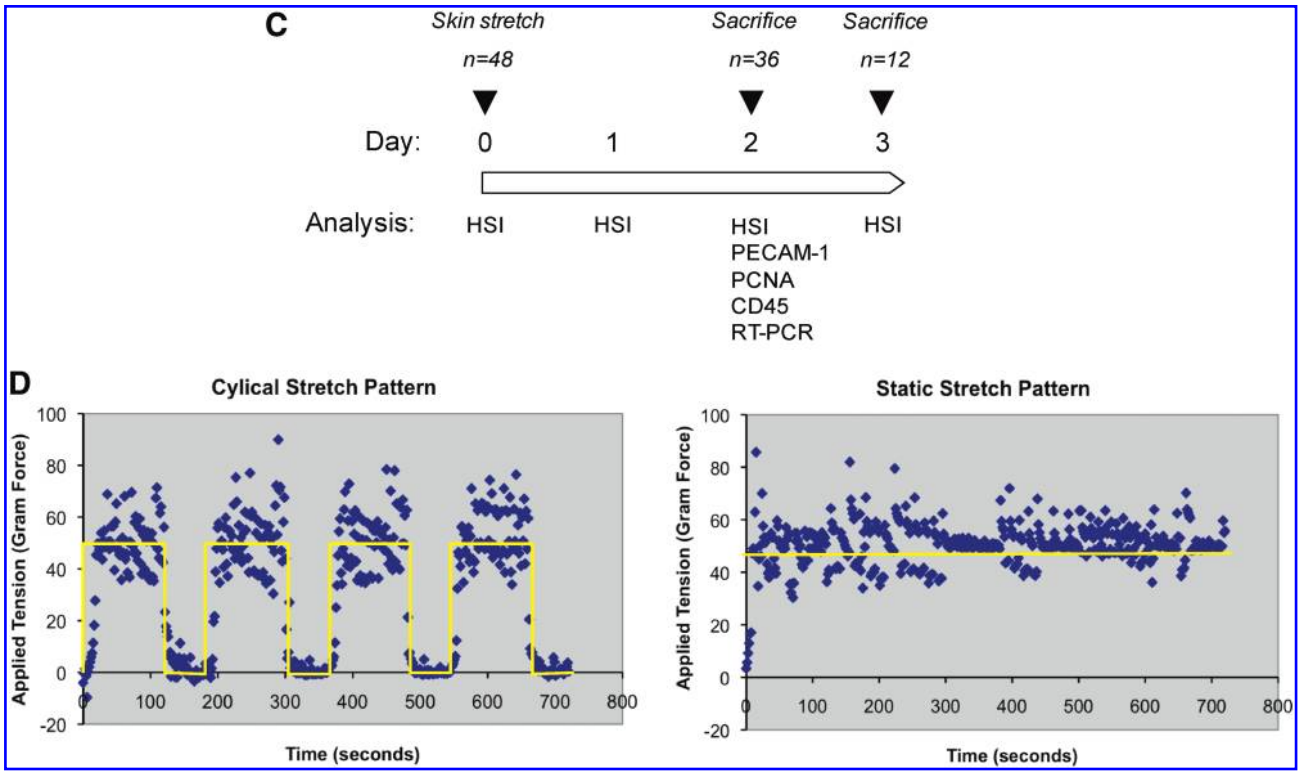
C
Skin stretch
n=48
Sacrifice
n=36
Sacrifice
n=12
Day:
0
1
2
3
Analysis:
HSI
HSI
HSI
PECAM-1
PCNA
CD45
RT-PCR
HSI
D
Cylical Stretch Pattern
Applied Tension (Gram Force)
Time (seconds)
Static Stretch Pattern
Applied Tension (Gram Force)
Time (seconds)

but no actual stretch applied. Mice were left free to move in their cages with water and food *ad libitum*. At the end of each stimulation, the device was carefully detached from the mouse. All animals were caged separately.

Mice from each group were sacrificed 2 days after stimulation. For each mouse, we harvested a full-thickness skin sample from the site of stimulation and a control sample from an area lateral to stretched skin. Each sample was comprised of skin, underlying subcutaneous tissue, and panniculus carnosus muscle and was cross sectioned along the longitudinal stretch axis. Samples were fixed in formalin, preserved in alcohol, and processed for histological slides. Immunohistochemical analysis of vessels, epidermal proliferation, and inflammation were detected by staining for platelet endothelial cell adhesion molecule-1, proliferating cell nuclear antigen (PCNA), and panleukocyte antigen (CD45),[17] respectively. Digital images were obtained from the middle of all stained skin sections and quantified by two observers blinded to the treatment arms. Vessel number (platelet endothelial cell adhesion molecule-1) was quantified using three sequential fields in the dermal layer at 10×magnification. Epidermal proliferation (PCNA) was quantified using three fields at 40×magnification and expressed as a ratio of PCNA positive to total nuclei in the epidermis. Inflammatory (CD45) cells were evaluated by counting positively stained cells in the dermis and epidermis using three fields at 40×magnification. Hair follicles were omitted from all quantifications. Vessel and proliferation rates were expressed as a ratio between the stimulated sample and its respective internal control. Any systemic effect produced by stretch of the target area was controlled by relative comparison to internal control skin so that only local effects in the stretched area were considered.

Real-time RT-PCR. We determined real-time RT-PCR expression of hypoxia-induced factor 1α (*HIF-1α*), vascular endothelial growth factor (*VEGF*), epidermal growth factor (*EGF*), transforming growth factor β1 (*TGF-β1*), and nerve growth factor (*NGF*). On day 2 after stretch, total RNA was extracted from 4 h cyclical ($n = 3$) and 4 h static ($n = 3$) groups along with corresponding unstretched internal control skin samples.

Fresh samples were washed, frozen, and sectioned. RNA was extracted using the RNeasy mini kit (Qiagen, Chatsworth, CA), and quantification was performed using the NanoDrop (NanoDrop Technologies, Wilmington, DE) method. We synthesized cDNA using a SuperScript III First-Strand Synthesis System for RT-PCR (Invitrogen Life Technologies, Carlsbad, CA). Total RNA was mixed with random hexamers and dNTP and then incubated. RT buffer, $MgCl_2$, DTT, RNaseOUT, and SuperScript III RT were added and incubated and cooled. Then, *Escherichia coli* RNase H was added and incubated.

Real-time RT-PCR was performed with primers designed for this study (Table 1) in an ABI Prism7300 system (Applied Biosystems, Foster City, CA) using RT^2 SYBR Green/ROX qPCR (SA Biosciences, Frederick, MD). Amplification of the cDNA was performed in triplicates, and a dissociation curve was generated with 28s ribosomal RNA as the endogenous control for normalization. To control for systemic effects, sample groups were each compared to its own respective internal control, producing a relative quantity (RQ). Comparative changes in gene expression were considered significant when the RQ error bars (RQ Max and Min), as determined by each sample's 95% confidence interval, did not overlap.

Hyperspectral imaging. For hyperspectral imaging (CombiVu-R System; HyperMed, Burlington, MA),[18] animals underwent 4 h cyclical stretch ($n = 5$), 4 h static stretch ($n = 4$), and sham ($n = 3$). Mice were imaged 1 h poststretch, and for the following 3 days. During each image acquisition, mice were anesthetized with pentobarbital (60 mg/kg IP), placed under the imaging device, and carefully secured with tape to prevent any movement. Imaging was performed in a dark room and under warm conditions.

Data were analyzed using two-dimensional image registration techniques by determining diffuse reflectance tissue spectra for each pixel within this collection of images. Mean oxy- (HT-Oxy) and deoxy-hemoglobin (HT-Deoxy) values were obtained from a 160-pixel-diameter region of the images of the stretched area by decomposition using standard spectra for HT-Oxy and HT-Deoxy. False color images were created to demonstrate tissue oxygenation spatially. HT-Oxy levels are associated with different colors and HT-Deoxy with different levels of brightness as depicted on the color bar provided alongside each image. Total hemoglobin (tHb) was calculated as the sum of HT-Oxy and HT-Deoxy. Oxygen saturation (StO_2) was calculated as HT-Oxy divided by tHb. All values were analyzed relative to the baseline prestretch image.

Statistical analyses. Values are expressed as means (±1 standard deviation) in text and figures unless otherwise noted. One-way analysis of variance at $p < 0.05$ level with

Table 1. Primers for Real-Time Reverse Transcriptase–Polymerase Chain Reaction

Gene	*GenBank ID*	*Sense*	*Antisense*
HIF-1α	NM_010431	5′-CAAGTCAGCAACGTGGAAGGT-3′	5′-CTGAGGTTGGTTACTGTTGGTATCA-3′
VEGF	M95200	5′-CACTGGACCCTGGCTTTACTGC-3′	5′-CGCCTTGGCTTGTCAC-3′
EGF	NM_010113	5′-CCAAACGCCGAAGACTTATCC-3′	5′-TGATCCTCAAACACGGCTAGAGA-3′
TGF-β1	NM_011577	5′-CACCATCCATGACATGAACC-3′	5′-TCATGTTGGACAACTGCTCC-3′
NGF	M35075	5′-GCCTCAAGCCAGTGAAATTAGG-3′	5′-ACGACCACAGGCCAAAACTC-3′
28s rRNA	X00525	5′-TTGAAAATCCGGGGGAGAG-3′	5′-ACATTGTTCCAACATGCCAG-3′

HIF-1α, hypoxia-induced factor 1α; *VEGF*, vascular endothelial growth factor; *EGF*, epidermal growth factor; *TGF-β1*, transforming growth factor β1; *NGF*, nerve growth factor.

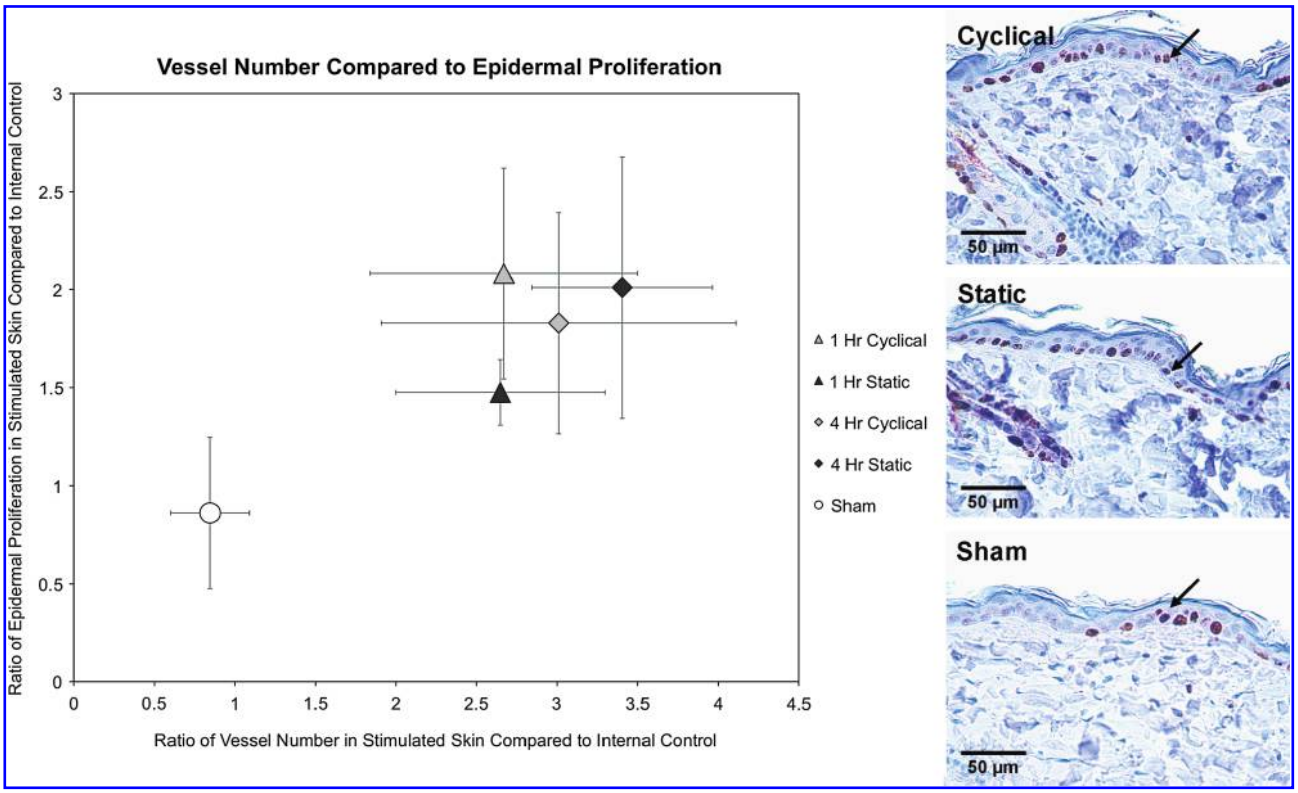

FIG. 2. (Left) Plot of vessel number and epidermal proliferation. For vessel number and epidermal proliferation, all stretch groups were significantly elevated compared to sham at day 2. Cyclical stretch proliferation was significantly higher than static stretch after 1 h of stretch. (Right) Proliferating cell nuclear antigen stains of epidermis in 4 h cyclical, static, and nonstretched skin. Arrows indicate proliferating cell nuclear antigen–positive cells. Color images available online at www.liebertonline.com/ten.

ad hoc Fischer's LSD tests were performed for comparisons of multiple groups using SPSS 13 (SPSS, Chicago, IL). For gene expression analysis, 95% confidence intervals for each sample were automatically determined by the ABI Prism7300 software (v 1.4; Applied Biosystems) and considered significant when intervals were not overlapping.

Results

Design and analysis of skin-stretching device

Finite element prediction of tissue response. Figure 1B shows the distribution of von Mises stress overlaid onto the model, deformed by the opposing displacements of adhesive pads A and B. The plots demonstrate symmetry in the stress field corresponding with the results expected from symmetric loading conditions. Stress concentrations were localized at the corners of the adhesive pads and along their proximal edges, indicating that these were regions of tissue to exclude. The large region of uniform stress between pads A and B showed that this region was suitable for analysis.

Reliability of tensile force application and absence of tissue damage. A careful review of each force recording verified that the device delivered the specified force patterns with minimal variation (Fig. 1D). Macroscopic examination of the stretched area skin showed no damage, but there was a small degree of inflammation and erythema limited to areas directly under the glued pads of the device. The skin, which showed temporary elongation, returned to original positioning after cessation of stretch without any noticeable mechanical creep. When inflammatory cells (CD45) were quantified, there were no differences between groups (data not shown).

In vivo *skin stretching and analysis of stretched skin*

Epidermal proliferation, angiogenesis, and growth factor expression. As both epidermal cellular proliferation and vasculature play integral roles in normal tissue growth, we have plotted epidermal proliferation in relation to vessel count in Figure 2. The baseline ratio is assumed to be 1.0 for nonstretched skin compared to internal control. There were no differences between sham skin and the baseline ratio, as well as no differences among the internal skin from each animal. Analysis for PCNA in the epidermis demonstrated that all four stretch groups had significantly elevated cellular proliferation over the sham group. Proliferation was significantly ($p = 0.042$) greater for 1 h cyclical (2.1 ± 0.5) compared to 1 h static stretch (1.5 ± 0.2). There were no differences between the 4 h cyclical and static stretch groups. Two days after stretching, vessel counts for cyclical and static stretch groups increased nearly threefold compared to the sham group ($p = 0.001$).

Comparisons of 95% confidence intervals for growth factor expression demonstrated significant *EGF* elevation in both cyclical and static stretch groups, with an 11-fold increase (RQ Max = 14.1, Min = 9.0) in the cyclical group (Fig. 3). RT-PCR

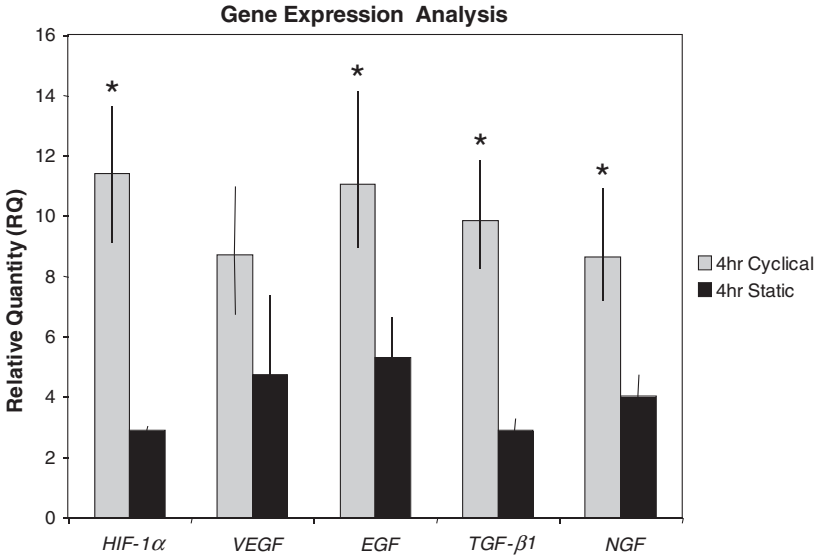

FIG. 3. Real-time RT-PCR for growth factors in cyclical and static stretch groups. All quantities are expressed relative to unstretched internal skin controls. Bars represent 95% confidence interval and groups were considered significantly different when bars were not overlapping as indicated by asterisks (*). Although all stretch groups were elevated from baseline, cyclically stretched skin was significantly more effective than continuous stretch for *HIF-1α, EGF, TGF-β1,* and *NGF* expression. TGF-*β1*, transforming growth factor β1; *NGF*, nerve growth factor.

for *VEGF* demonstrated a nearly ninefold upregulation (RQ Max = 11.0, Min = 6.7) for cyclically stretched skin compared to baseline, whereas statically stretched skin showed only 4.7-fold increase (RQ Max = 7.3, Min = 3.0). Cyclical stretch resulted in 8.6-fold (RQ Max = 11.9, Min = 8.3) and 9.8-fold (RQ Max = 10.9, Min = 7.2) increases in *TGF-β1* and *NGF* expression, respectively. Continuously stretched skin was significantly less effective in upregulating *TGF-β1* and *NGF* with 2.9-fold (RQ Max = 3.3, Min = 2.3) and 4.0-fold (RQ Max = 4.7, Min = 2.9) increases, respectively.

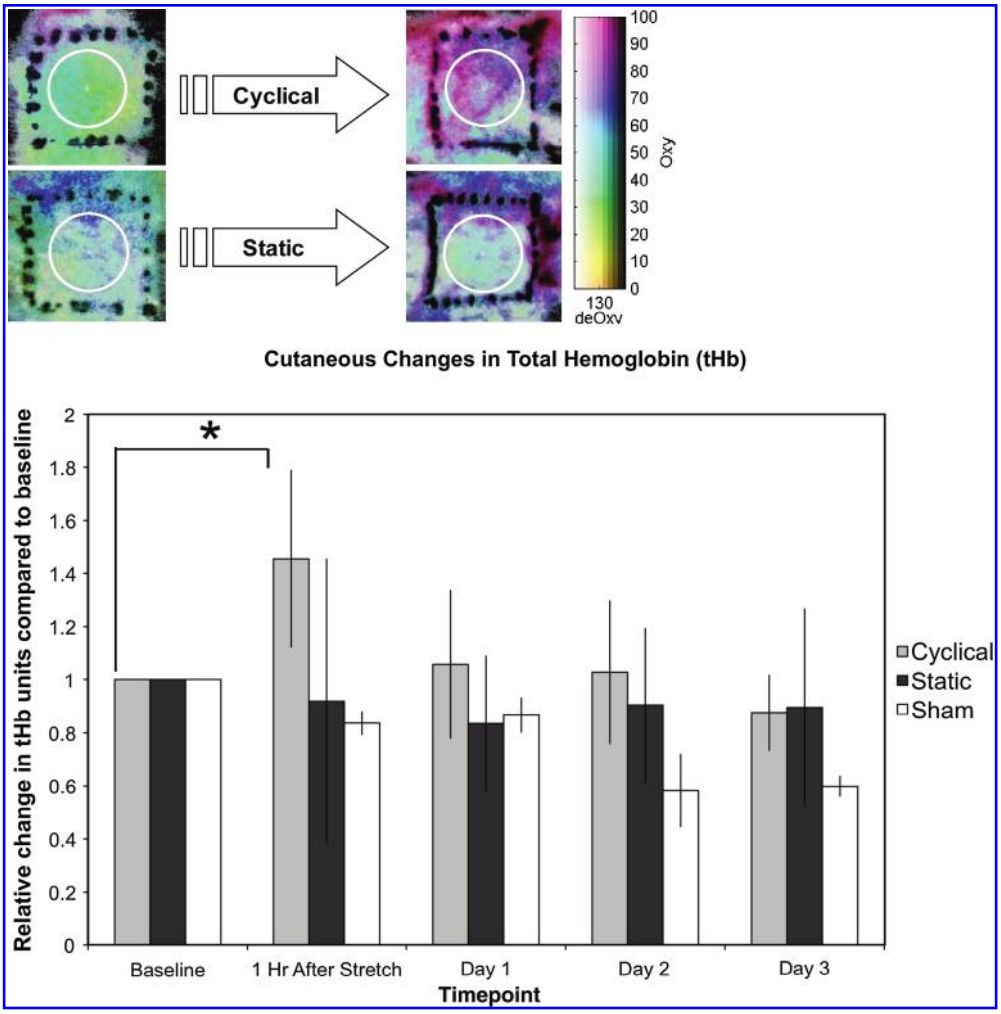

FIG. 4. (Above) Hyperspectral images of 4 h cyclically and statically stretched skin. The local inflammation due to device attachment is outside of the analyzed skin area. (Below) Plot of total hemoglobin in stretched and sham skin. Only cyclically stretched skin led to a significant increase from baseline as indicated by asterisk (*) ($p = 0.007$). Color images available online at www.liebertonline.com/ten.

Tissue hypoxia during active stretch. On day 2 after stretch, RT-PCR analysis for *HIF-1α* showed a 11.4-fold gene expression upregulation (RQ Max = 13.6, Min = 9.1) in cyclically stretched skin over baseline, and a significantly smaller 2.9-fold elevation (RQ Max = 3.4, Min = 2.7) in statically stretched skin (Fig. 3).

Cutaneous perfusion. Using hyperspectral imaging, there was a significant 50% increase in HT-Oxy 1 h following 4 h of cyclical stretch when compared to its baseline ($p = 0.002$). This returned to slightly below baseline in the following days. HT-Deoxy did not demonstrate any statistical differences between days regardless of stimulation group. The cyclical stretch group exhibited a significant 46% increase in tHb compared to its prestretch baseline ($p = 0.007$), returning to baseline in the following days. The static stretch group did not have significant differences in tHb between days (Fig. 4). There was no change in StO_2 for any group.

Discussion

In vivo *application of mechanical forces for skin tissue engineering*

Despite numerous studies in musculoskeletal[19–21] and cardiovascular[22–24] tissue engineering, mechanotransduction has not been widely studied in skin tissue engineering. In normal growth and development, skin expands to cover the growing skeleton and soft tissues, and skin is constantly subjected to tension due to the body's movements. Application of mechanical forces is necessary to simulate the naturally occurring conditions for optimal skin growth and regeneration.

In reconstructive surgery, expanded skin due to pregnancy,[25,26] implanted tissue expanders,[27,28] or simple tape[29] has been used. We previously demonstrated that cell proliferation and vascular remodeling occur in stretched skin[11] and suggest that these biological effects can be modulated by skin-stretching devices. Because conventional skin-growing strategies rely on static force application and are time consuming, repetitive stimulation may accelerate the growth process. A reliable model for *in vivo* studies of cyclical stretch on skin is lacking.

Analysis of the in vivo *biological effects of the stretching device*

Our prototype device demonstrates that the application of cyclical tensile force is a feasible approach to the acceleration of skin growth. We stretched at an amplitude of 50 gm-f based on our previous study, which demonstrated that this force is great enough to stimulate growth yet lies within limits to avoid tissue injury.[11] For this study, we chose to compare the shortest cycle timing reliably produced by the device (2 min on/1 min off) to the longest cycle (continuous

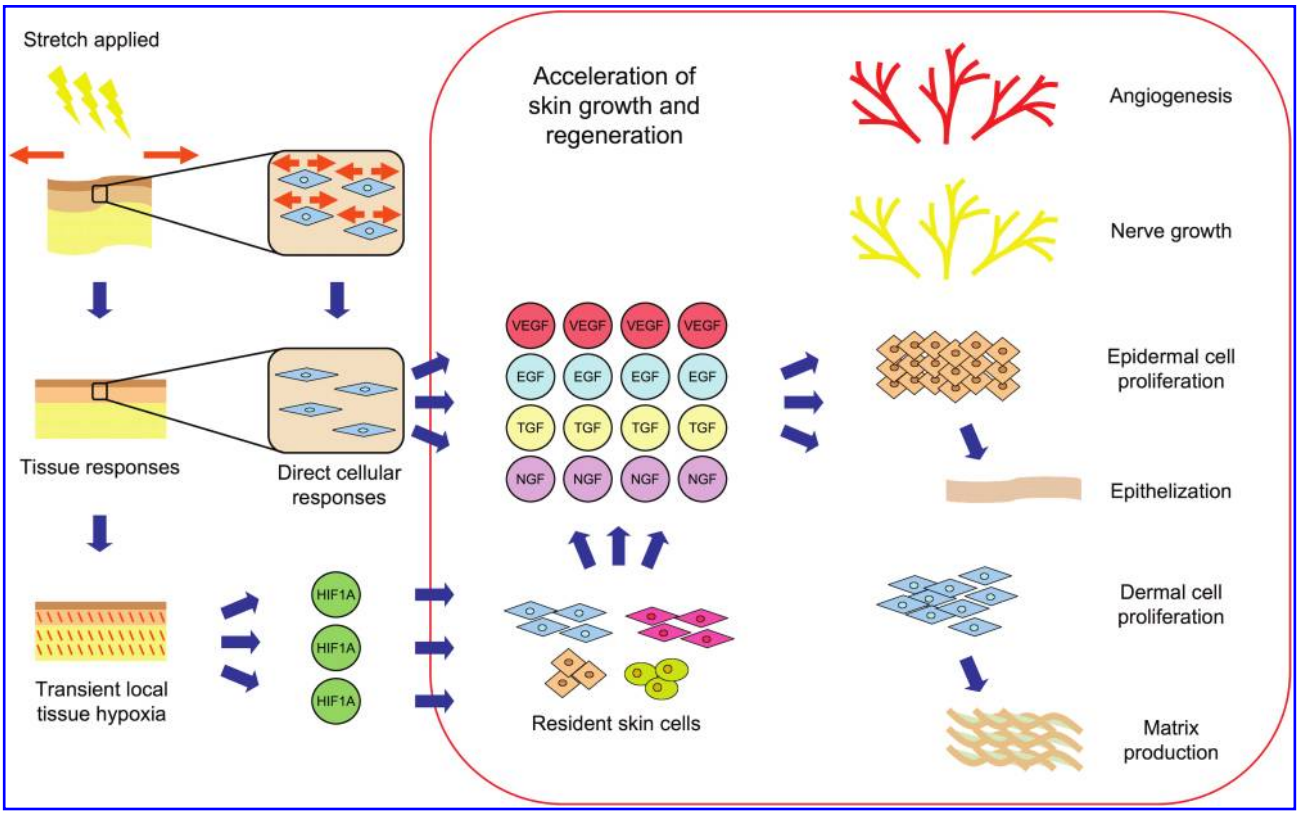

FIG. 5. Proposed parallel mechanisms for skin growth. Based on our results and previous studies, it is likely that there are mechanisms promoting tissue growth on both the cellular as well as the macroscopic level. Previous studies have implicated the role of induced cellular growth through direct stimulation of the cell and related mechanotransduction pathways. Our results support these theories, but also suggests that transient hypoxia may also be a powerful stimulus for promoting tissue growth. Color images available online at www.liebertonline.com/ten.

stretch). Immunohistochemical analysis for epidermal proliferation showed a strong response to cyclical stretch after only 1 h of stimulation, and significantly greater *EGF* elevation occurred in the cyclical stretch group. These results support previous suggestions that cyclical force is better for stimulating tissue growth than static force.[30]

Our previous gene chip analysis performed on stretched rat ear tissue suggested that hypoxia played a role in the cellular changes observed.[13] Lew and Fuseler hypothesized that increased vascularity during pulsed tissue expansion may be attributable to temporary hypoxia.[30] Our RT-PCR analysis for *HIF-1α,* a known transcriptional factor for both hypoxia and angiogenesis,[31] demonstrated a 11-fold increase 2 days after cyclical stretch. This robust *HIF-1α* (and downstream *VEGF*) response to cyclical stretch may be due to the repeated high-frequency stimulation of transient hypoxia. *HIF-1α* is not only a known promoter of *VEGF*,[32] but also has shown to increase the expression of *EGF,* which is consistent with our results.[33] Hypoxia has also been associated with elevations in *TGF-β1*[34] and *NGF*[35] expression, which is supported by our current study. Due to the complex nature of *in vivo* models, additional mechanisms other than temporary hypoxia may account for increased tissue response. We propose that in addition to transient local hypoxia, mechanotransduction related are also activated in parallel (Fig. 5).

Further, adequate blood flow is essential to normal tissue growth, and due to the *in vivo* nature of our model, we were able to analyze the cutaneous perfusion after stretching. We employed the use of hyperspectral imaging to quantify changes in perfusion after completion of skin stretch. We demonstrated that cyclically stretched skin led to increased tissue oxygenation, suggesting that cyclical stimulation may confer increased tissue oxygenation and improve skin viability. Together with the residual upregulation of *HIF-1α,* these results suggest that hypoxia is transiently induced during active tension, but re-perfusion occurs when stretching ceases.

Directions for future skin tissue engineering

Our prototype device has demonstrated that cyclical force application enhances epidermal proliferation, vessel growth, and overall cutaneous perfusion. Waveform-specific mechanical loads may accelerate tissue growth by maximizing cellular signals produced during repeated cycles of temporary hypoxia in addition to pathways activated by mechanotransduction. However, the potential for re-perfusion injury or tissue ischemia should be evaluated further.

Future study of force waveforms is warranted as the parameters for optimal skin growth have yet to be defined. Our prototype provides a reliable and effective model for *in vivo* study of the effects of cyclical stretch, but future modifications that enable shorter cycle intervals will be useful for exploring these parameters. An *in vitro* system that could efficiently compare specific waveforms used with this device would be helpful in future determinations of possible optimal waveforms for correlation *in vivo*. In addition, further *in vivo* analysis of the possible activated mechanotransduction signaling pathways, such as extracellular signal–regulated kinase,[36] c-Jun N-terminal kinase,[36] and phosphatidylinositol 3-kinase/Akt,[37] should be performed on both the cellular and tissue levels in skin. For clinical correlation, we hope to use a comparable device in human studies in the near future to accelerate dermatogenesis.[29] Our device concept provides opportunities to study not only *in vivo* stretching of natural skin, but also potential waveforms that accelerate growth of skin substitutes and development of cell therapies for skin healing and regeneration.

Acknowledgments

The authors would like to thank George Younan, M.D. for his excellent technical assistance in the collection and preparation of the data. Additionally, the authors would like to recognize the support of Sean Oakes and the Moore Surgical Laboratory, without which this project would not have been possible.

Disclosure Statement

Dr. Schomacker is an employee of HyperMed, a medical device company located in Burlington, MA, that is developing and commercializing hyperspectral imaging technology. Dr. Schomacker owns stock in the company.

References

1. Darling, E.M., and Athanasiou, K.A. Articular cartilage bioreactors and bioprocesses. Tissue Eng **9,** 9, 2003.
2. Gilbert, T.W., Stewart-Akers, A.M., Sydeski, J., Nguyen, T.D., Badylak, S.F., and Woo, S.L. Gene expression by fibroblasts seeded on small intestinal submucosa and subjected to cyclic stretching. Tissue Eng **13,** 1313, 2007.
3. Saris, D.B., Mukherjee, N., Berglund, L.J., Schultz, F.M., An, K.N., and O'Driscoll, S.W. Dynamic pressure transmission through agarose gels. Tissue Eng **6,** 531, 2000.
4. Wood, M.A., Yang, Y., Thomas, P.B., and Haj, A.J. Using dihydropyridine-release strategies to enhance load effects in engineered human bone constructs. Tissue Eng **12,** 2489, 2006.
5. Hu, J.C., and Athanasiou, K.A. The effects of intermittent hydrostatic pressure on self-assembled articular cartilage constructs. Tissue Eng **12,** 1337, 2006.
6. Miyanishi, K., Trindade, M.C., Lindsey, D.P., Beaupre, G.S., Carter, D.R., Goodman, S.B., Schurman, D.J., and Smith, R.L. Effects of hydrostatic pressure and transforming growth factor-beta 3 on adult human mesenchymal stem cell chondrogenesis *in vitro.* Tissue Eng **12,** 1419, 2006.
7. Stockbridge, L.L., and French, A.S. Stretch-activated cation channels in human fibroblasts. Biophys J **54,** 187, 1988.
8. Matthews, B.D., Overby, D.R., Mannix, R., and Ingber, D.E. Cellular adaptation to mechanical stress: role of integrins, Rho, cytoskeletal tension and mechanosensitive ion channels. J Cell Sci **119 (Pt 3),** 508, 2006.
9. Wang, N., Butler, J.P., and Ingber, D.E. Mechanotransduction across the cell surface and through the cytoskeleton. Science **260,** 1124, 1993.
10. Wu, Z., Wong, K., Glogauer, M., Ellen, R.P., and McCulloch, C.A. Regulation of stretch-activated intracellular calcium transients by actin filaments. Biochem Biophys Res Commun **261,** 419, 1999.
11. Pietramaggiori, G., Liu, P., Scherer, S.S., Kaipainen, A., Prsa, M.J., Mayer, H., Newalder, J., Alperovich, M., Mentzer, S.J., Konerding, M.A., Huang, S., Ingber, D.E., and Orgill, D.P. Tensile forces stimulate vascular remodeling and epidermal cell proliferation in living skin. Ann Surg **246,** 896, 2007.

12. Chin, M.S., Lancerotto, L., Helm, D.L., Dastouri, P., Prsa, M.J., Ottensmeyer, M., Akaishi, S., Orgill, D.P., and Ogawa, R. Analysis of neuropeptides in stretched skin. Plast Reconstr Surg **124,** 102, 2009.
13. Saxena, V., Orgill, D., and Kohane, I. A set of genes previously implicated in the hypoxia response might be an important modulator in the rat ear tissue response to mechanical stretch. BMC Genomics **8,** 430, 2007.
14. Takei, T., Rivas-Gotz, C., Delling, C.A., Koo, J.T., Mills, I., McCarthy, T.L., Centrella, M., and Sumpio, B.E. Effect of strain on human keratinocytes *in vitro*. J Cell Physiol **173,** 64, 1997.
15. Ingber, D.E., Prusty, D., Sun, Z., Betensky, H., and Wang, N. Cell shape, cytoskeletal mechanics, and cell cycle control in angiogenesis. J Biomech **28,** 1471, 1995.
16. Von Offenberg Sweeney, N., Cummins, P.M., Cotter, E.J., Fitzpatrick, P.A., Birney, Y.A., Redmond, E.M., and Cahill, P.A. Cyclic strain-mediated regulation of vascular endothelial cell migration and tube formation. Biochem Biophys Res Commun **329,** 573, 2005.
17. Scherer, S.S., Pietramaggiori, G., Mathews, J.C., Prsa, M.J., Huang, S., and Orgill, D.P. The mechanism of action of the vacuum-assisted closure device. Plast Reconstr Surg **122,** 786, 2008.
18. Greenman, R.L., Panasyuk, S., Wang, X., Lyons, T.E., Dinh, T., Longoria, L., Giurini, J.M., Freeman, J., Khaodhiar, L., and Veves, A. Early changes in the skin microcirculation and muscle metabolism of the diabetic foot. Lancet **366,** 1711, 2005.
19. Kreke, M.R., and Goldstein, A.S. Hydrodynamic shear stimulates osteocalcin expression but not proliferation of bone marrow stromal cells. Tissue Eng **10,** 780, 2004.
20. Waldman, S.D., Spiteri, C.G., Grynpas, M.D., Pilliar, R.M., and Kandel, R.A. Long-term intermittent compressive stimulation improves the composition and mechanical properties of tissue-engineered cartilage. Tissue Eng **10,** 1323, 2004.
21. Detamore, M.S., and Athanasiou, K.A. Use of a rotating bioreactor toward tissue engineering the temporomandibular joint disc. Tissue Eng **11,** 1188, 2005.
22. Williams, C., and Wick, T.M. Perfusion bioreactor for small diameter tissue-engineered arteries. Tissue Eng **10,** 930, 2004.
23. Latimer, D.C., Roth, B.J., and Parker, K.K. Analytical model for predicting mechanotransduction effects in engineered cardiac tissue. Tissue Eng **9,** 283, 2003.
24. Narita, Y., Hata, K., Kagami, H., Usui, A., Ueda, M., and Ueda, Y. Novel pulse duplicating bioreactor system for tissue-engineered vascular construct. Tissue Eng **10,** 1224, 2004.
25. Riordan, C., Budny, P., and Regan, P. Pregnancy as an autologous tissue expander for closure of an abdominal-wall defect. Br J Plast Surg **56,** 64, 2003.
26. Elwood, E.T., Ingram, W.L., and Carlson, G.W. Pregnancy as a tissue expander in the repair of a massive ventral hernia. Ann Plast Surg **45,** 431, 2000.
27. Manders, E.K., Schenden, M.J., Furrey, J.A., Hetzler, P.T., Davis, T.S., and Graham, W.P., 3rd. Soft-tissue expansion: concepts and complications. Plast Reconstr Surg **74,** 493, 1984.
28. Gao, J.H., Ogawa, R., Hyakusoku, H., Lu, F., Hu, Z.Q., Jiang, P., Yang, L., and Feng, C. Reconstruction of the face and neck scar contractures using staged transfer of expanded "Super-thin flaps." Burns **33,** 760, 2007.
29. Daya, M., and Nair, V. Traction-assisted dermatogenesis by serial intermittent skin tape application. Plast Reconstr Surg **122,** 1047, 2008.
30. Lew, D., and Fuseler, J.W. The effect of pulsed expansion of subfascially placed expanders on the extent and duration of mitosis in the capsule and rat integument. J Oral Maxillofac Surg **51,** 154, 1993.
31. Yamakawa, M., Liu, L.X., Date, T., Belanger, A.J., Vincent, K.A., Akita, G.Y., Kuriyama, T., Cheng, S.H., Gregory, R.J., and Jiang, C. Hypoxia-inducible factor-1 mediates activation of cultured vascular endothelial cells by inducing multiple angiogenic factors. Circ Res **93,** 664, 2003.
32. Schultz, K., Fanburg, B.L., and Beasley, D. Hypoxia and hypoxia-inducible factor-1alpha promote growth factor-induced proliferation of human vascular smooth muscle cells. Am J Physiol Heart Circ Physiol **290,** H2528, 2006.
33. Elson, D.A., Ryan, H.E., Snow, J.W., Johnson, R., and Arbeit, J.M. Coordinate up-regulation of hypoxia inducible factor (HIF)-1alpha and HIF-1 target genes during multi-stage epidermal carcinogenesis and wound healing. Cancer Res **60,** 6189, 2000.
34. Falanga, V., Qian, S.W., Danielpour, D., Katz, M.H., Roberts, A.B., and Sporn, M.B. Hypoxia upregulates the synthesis of TGF-beta 1 by human dermal fibroblasts. J Invest Dermatol **97,** 634, 1991.
35. Lorez, H., Keller, F., Ruess, G., and Otten, U. Nerve growth factor increases in adult rat brain after hypoxic injury. Neurosci Lett **98,** 339, 1989.
36. Kook, S.H., Hwang, J.M., Park, J.S., Kim, E.M., Heo, J.S., Jeon, Y.M., and Lee, J.C. Mechanical force induces type I collagen expression in human periodontal ligament fibroblasts through activation of ERK/JNK and AP-1. J Cell Biochem **106,** 1060, 2009.
37. Dogra, C., Changotra, H., Wergedal, J.E., and Kumar, A. Regulation of phosphatidylinositol 3-kinase (PI3K)/Akt and nuclear factor-kappa B signaling pathways in dystrophin-deficient skeletal muscle in response to mechanical stretch. J Cell Physiol **208,** 575, 2006.

Address correspondence to:
Dennis P. Orgill, M.D., Ph.D.
Division of Plastic Surgery
Tissue Engineering and Wound Healing Laboratory
Harvard Medical School
Brigham and Women's Hospital
75 Francis St.
Boston, MA 02115

E-mail: dorgill@partners.org

Received: March 17, 2009
Accepted: July 14, 2009
Online Publication Date: September 17, 2009

This article has been cited by:

1. Sean Kirkpatrick, Stephen Matcher, Stephen MorganMacroscopic Imaging in Regenerative Medicine 383-402. [CrossRef]
2. E.M. Valesky, R. Kaufmann, M. Meissner. 2013. Besondere Indikationen der Vakuumversiegelungstherapie in der Dermatochirurgie. *Der Hautarzt* **64**:8, 585-591. [CrossRef]
3. Chenyu Huang, Kunio Miyazaki, Satoshi Akaishi, Atsushi Watanabe, Hiko Hyakusoku, Rei Ogawa. 2013. Biological effects of cellular stretch on human dermal fibroblasts. *Journal of Plastic, Reconstructive & Aesthetic Surgery* . [CrossRef]
4. Michael S. Chin, Brian B. Freniere, Caitlin F. Bonney, Luca Lancerotto, Jonathan H. Saleeby, Yuan-Chyuan Lo, Dennis P. Orgill, Thomas J. Fitzgerald, Janice F. Lalikos. 2013. Skin Perfusion and Oxygenation Changes in Radiation Fibrosis. *Plastic and Reconstructive Surgery* **131**:4, 707-716. [CrossRef]
5. Kristine C. Rustad, Victor W. Wong, Geoffrey C. Gurtner. 2013. The role of focal adhesion complexes in fibroblast mechanotransduction during scar formation. *Differentiation* . [CrossRef]
6. Luca Lancerotto, Lauren R. Bayer, Dennis P. Orgill. 2012. Mechanisms of action of microdeformational wound therapy. *Seminars in Cell & Developmental Biology* **23**:9, 987-992. [CrossRef]
7. Moris Topaz, Narin-Nard Carmel, Adi Silberman, Ming Sen Li, Yong Zhong Li. 2012. The TopClosure® 3S System, for skin stretching and a secure wound closure. *European Journal of Plastic Surgery* **35**:7, 533-543. [CrossRef]
8. Rei Ogawa, Kazuhisa Okai, Fumio Tokumura, Kazuyuki Mori, Yasutaka Ohmori, Chenyu Huang, Hiko Hyakusoku, Satoshi Akaishi. 2012. The relationship between skin stretching/contraction and pathologic scarring: The important role of mechanical forces in keloid generation. *Wound Repair and Regeneration* n/a-n/a. [CrossRef]
9. Michael S. Chin, Brian B. Freniere, Yuan-Chyuan Lo, Jonathan H. Saleeby, Stephen P. Baker, Heather M. Strom, Ronald A. Ignotz, Janice F. Lalikos, Thomas J. Fitzgerald. 2012. Hyperspectral imaging for early detection of oxygenation and perfusion changes in irradiated skin. *Journal of Biomedical Optics* **17**:2, 026010. [CrossRef]
10. Rei Ogawa. 2011. Mechanobiology of scarring. *Wound Repair and Regeneration* **19**, s2-s9. [CrossRef]
11. Franco Bassetto, Luca Lancerotto, Roberto Salmaso, Laura Pandis, Giorgio Pajardi, Mauro Schiavon, Cesare Tiengo, Vincenzo Vindigni. 2011. Histological evolution of chronic wounds under negative pressure therapy. *Journal of Plastic, Reconstructive & Aesthetic Surgery* . [CrossRef]
12. Rodolpho Alberto Bussolaro, Elvio Bueno Garcia, Maria Teresa Zanella, Lydia Masako Ferreira. 2011. Impaired Abdominal Skin Sensory Function in Morbid Obesity and After Bariatric Surgery. *Obesity Surgery* . [CrossRef]
13. Peter A. Galie, Jan P. Stegemann. 2011. Simultaneous Application of Interstitial Flow and Cyclic Mechanical Strain to a Three-Dimensional Cell-Seeded Hydrogel. *Tissue Engineering Part C: Methods* **17**:5, 527-536. [Abstract] [Full Text HTML] [Full Text PDF] [Full Text PDF with Links]
14. Rei Ogawa, Satoshi Akaishi, Chenyu Huang, Teruyuki Dohi, Masayo Aoki, Yasutaka Omori, Sachiko Koike, Kyoko Kobe, Masataka Akimoto, Hiko Hyakusoku. 2011. Clinical Applications of Basic Research that Shows Reducing Skin Tension Could Prevent and Treat Abnormal Scarring: The Importance of Fascial/Subcutaneous Tensile Reduction Sutures and Flap Surgery for Keloid and Hypertrophic Scar Reconstruction. *Journal of Nippon Medical School* **78**:2, 68-76. [CrossRef]